Improved near-infrared transparency in sputtered In 2 O 3 -based transparent conductive oxide thin films by Zr-doping

T. Koida and M. Kondo

Citation: Journal of Applied Physics **101**, 063705 (2007); doi: 10.1063/1.2711768
View online: http://dx.doi.org/10.1063/1.2711768
View Table of Contents: http://scitation.aip.org/content/aip/journal/jap/101/6?ver=pdfcov
Published by the AIP Publishing

Improved near-infrared transparency in sputtered In_2O_3-based transparent conductive oxide thin films by Zr-doping

T. Koida[a] and M. Kondo
Research Center for Photovoltaics, National Institute of Advanced Industrial Science and Technology (AIST), Central 2, Umezono 1-1-1, Tsukuba Ibaraki 305-8568, Japan

(Received 20 October 2006; accepted 17 January 2007; published online 23 March 2007)

Transparent conductive Zr-doped In_2O_3 ($In_{2-2x}Zr_{2x}O_3$) films were deposited on glasses by sputtering method. High mobility of over 80 $cm^2/V\,s$ was achieved under a carrier density of $1.3-2.9\times10^{20}$ cm^{-3} at Zr concentrations (x) of 0.014–0.022, and the film at $x=0.022$ showed the lowest resistivity of 2.6×10^{-4} Ω cm. Reflecting the high mobility and the low carrier density, the transparency extended from the visible to the near-infrared (NIR) wavelength region with reduced magnitude of the free-carrier absorption. The results indicate that Zr-doped In_2O_3 films have a performance advantage for applications that require high conductivity and transparency in NIR wavelength region. © *2007 American Institute of Physics*. [DOI: 10.1063/1.2711768]

I. INTRODUCTION

Near-infrared (NIR)-transparent conductive oxide (TCO) films are attracting attention because of the possibility of widening spectral sensitivity of thin-film solar cells from the visible to the NIR wavelength region. Indeed, an optical loss in the NIR wavelength region due to the free-carrier absorption in conventional TCO electrodes are drawing attention in Si or $CuIn_{1-x}Ga_xSe_2$-based multijunction solar cells, which are expected to be near-future thin-film solar cells with high conversion efficiency. According to the Drude model, the increase of the transparency window to the NIR wavelength region without compromising the conductivity can only be obtained by increasing the mobility with decreasing carrier density.

So far, Sn-doped In_2O_3 (ITO) has been widely used as transparent electrodes, because ITO films have high transparency to visible light and low resistivity can be easily fabricated at relatively low temperature. Generally, Sn has been regarded as the only useful dopant for In_2O_3; however, Groth reported high-mobility Ti- and Zr-doped In_2O_3 thin films grown on glasses by spray method in 1966, and high mobility of 120 and 170 $cm^2/V\,s$ under the carrier density of 1×10^{20} and 8×10^{19} cm^{-3} was obtained for Ti- and Zr-doped In_2O_3 films, respectively.[1] Recently, high-mobility and NIR-transparent In_2O_3 thin films on glasses have been reported by doping metals such as Mo,[2–5] Ti,[5,6] and W,[7,8] and demonstrated as a transparent electrode for a solar cell having sensitivity in the visible to the NIR wavelength region.[9] These films also showed high mobility (>80 $cm^2/V\,s$) under the carrier density larger than 10^{20} cm^{-3}, and the values of mobility are factors of 2–3 greater than those of ITO. We have also reported high-mobility ($100-110$ $cm^2/V\,s$) Zr-doped In_2O_3 single-crystalline films[10] with carrier density of approximately 1×10^{20} cm^{-3}, which were obtained by Zr-doping to the high-quality In_2O_3 using pulsed laser deposition (PLD) method.[11]

In this article, the deposition of Zr-doped In_2O_3 on glasses by sputtering method is described, and the structural, electrical, and optical properties of the films are investigated. The influences of Zr-doping concentration on the properties are discussed with comparison to Zr-doped In_2O_3 single-crystalline films.

II. EXPERIMENT

$In_{2-2x}Zr_{2x}O_3$ thin films were grown on glasses (Corning 1737) by radio frequency (rf) magnetron cosputtering system (EIKO Engineering Co.) as illustrated in Fig. 1. As source materials, In_2O_3 and $In_{1.9}Zr_{0.1}O_3$ ceramic targets with a diameter of 3 in. were used, which were aiming at the substrate from opposite directions with an angle of 60° to the substrate plane. The substrate was rotated for uniform film deposition. The base pressure of the deposition chamber was below 5×10^{-6} Pa, and ambient pressure during growth was 0.5 Pa. Sputtering gases were O_2 and Ar with $O_2/(Ar+O_2)$ ratio of 0.0038. Each rf power ranged from 0 to 200 W, keeping the total growth rate at approximately 0.12 nm/s, which was

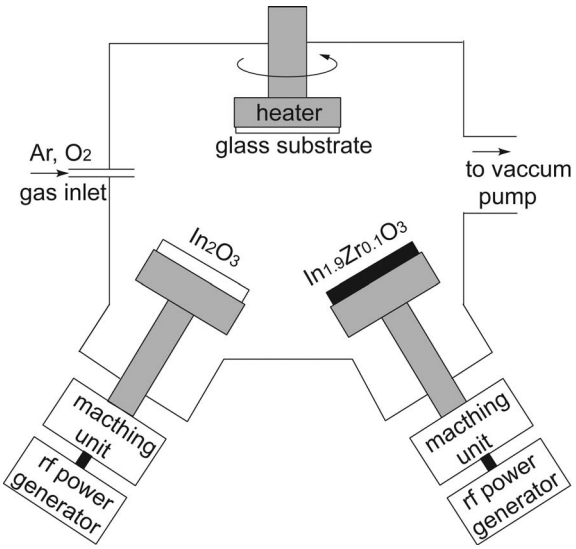

FIG. 1. Schematic illustration of experimental setup for cosputtering.

[a]Electronic mail: t-koida@aist.go.jp

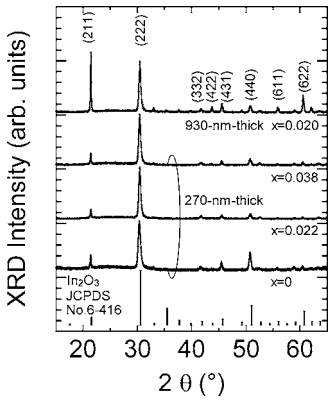

FIG. 2. XRD $\theta-2\theta$ profiles for $In_{2-2x}Zr_{2x}O_3$ films on glasses. Stick pattern of In_2O_3 (JCPDS No. 6–416) is also shown for comparison.

monitored by a quartz crystal oscillator. Typical thickness of the $In_{2-2x}Zr_{2x}O_3$ films was approximately 270 nm thick; a 930 nm thick film was also deposited in order to investigate the effects of film thickness on structural and electrical properties. The substrate temperature was 450 °C, and, after the growth, the substrate was cooled down at the rate of 10 °C/min. The Zr composition (x) of the films was analyzed by electron dispersive x-ray analysis. The crystal structure was analyzed by x-ray diffraction (XRD). Electrical resistivity, carrier density, and Hall mobility were measured using van der Pauw's method. Transmittance and reflectance spectra were measured by ultraviolet/visible/NIR spectrophotometers.

III. RESULTS AND DISCUSSION

$\theta-2\theta$ XRD patterns of $In_{2-2x}Zr_{2x}O_3$ thin films grown on glasses are shown in Fig. 2. For all the films, the patterns can be indexed based on the unit cell of a cubic In_2O_3 (JCPDS No. 6–416). As can be clearly seen in the 930 nm thick film, preferred orientation growth to ⟨211⟩ occurred, and no other impurity phases were observed, indicating that solid solution occurred in this composition range. The lattice constants as a function of x are shown in Fig. 3(a), which were calculated from (222), (332), (431), (440), and (622) peaks using the least-squares method. The lattice constants were almost constant and independent of x, probably due to the similar ionic radius between In^{3+} (80 p.m.) and Zr^{4+} (72 p.m.). The lattice constants of 270 nm thick films were larger than that of the bulk In_2O_3; however, it approached the value with increasing thickness. On the other hand, the crystalline size of the films estimated from full width at half maximum values of (211) and (222) peaks using Scherrer's equation were also independent of x, as shown in Fig. 3(b). Also, the crystalline size oriented to the ⟨211⟩ direction increased with thickness, indicating preferred orientation to ⟨211⟩ with film thickness as mentioned above.

Figure 4 shows the electrical resistivity, carrier density, and Hall mobility of the $In_{2-2x}Zr_{2x}O_3$ films as a function of x. $In_{2-2x}Zr_{2x}O_3$ single-crystalline films fabricated by PLD (Ref. 10) are also shown for comparison. The dotted line is the expected carrier density assuming that all the Zr^{4+} ions substitute In^{3+} sites and generate one electron per Zr. The behavior of electrical property of sputtered $In_{2-2x}Zr_{2x}O_3$ films as a function of x can be separated into three stages as follows: (i) In the range of $x \lesssim 0.01$, the carrier density decreased with gradual increase in mobility. (ii) In the range of $0.01 \lesssim x \lesssim 0.025$, the carrier density steeply increased while maintaining relatively high mobility ($\sim 80\ cm^2/V\ s$). (iii) In the range of $x \gtrsim 0.025$, the carrier density saturated and slightly decreased with gradual decrease in mobility. Accordingly, low resistivity ($\sim 2.5\times10^{-4}\ \Omega$ cm) was realized at $x \sim 0.02$. The value of the resistivity is similar to those of commercial ITO films; however, due to their substantially

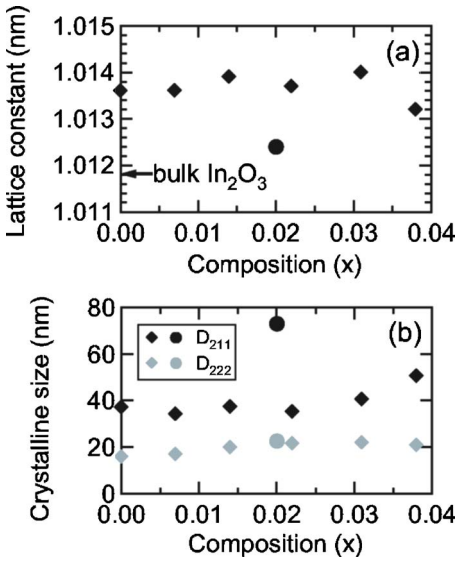

FIG. 3. (a) Lattice constants of $In_{2-2x}Zr_{2x}O_3$ polycrystalline films as a function of Zr composition (x). (b) Crystalline size of the films estimated from full width at half maximum values of (211) and (222) peaks using Scherrer's equation. The data of 930 nm thick film at $x=0.020$ are also shown as closed circles.

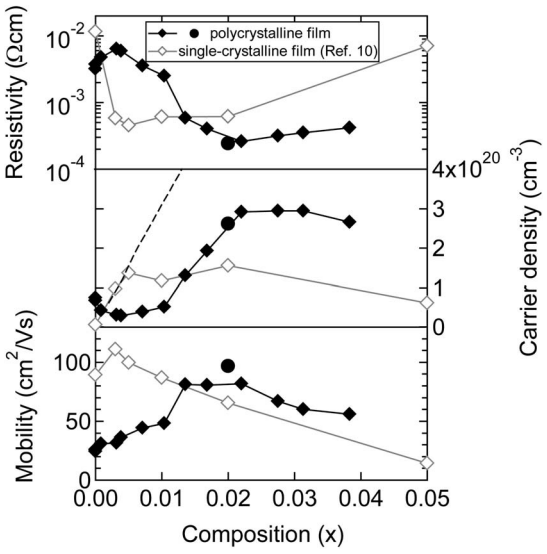

FIG. 4. Resistivity, carrier density, and Hall mobility of $In_{2-2x}Zr_{2x}O_3$ films as a function of Zr composition (x). The dotted line denotes the expected carrier density assuming that all the Zr^{4+} ions substitute In^{3+} sites and generate one electron per Zr. The data of 930 nm thick sputtered film at $x=0.020$, and single-crystalline films (after Ref. 10) are also shown as closed circles and open diamonds, respectively.

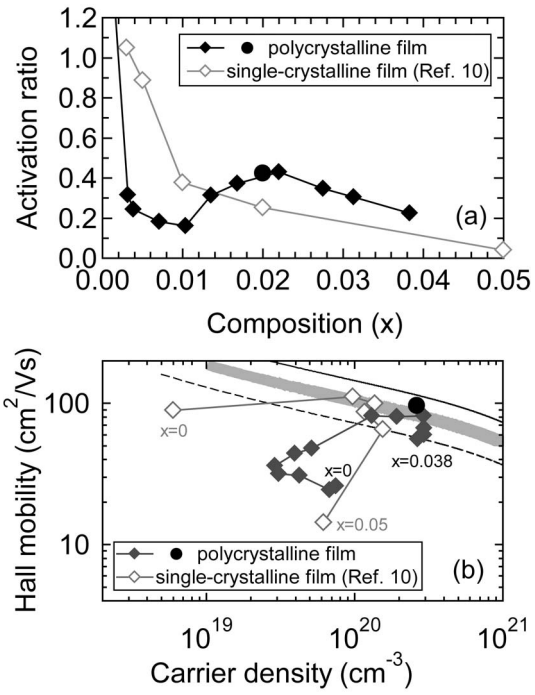

FIG. 5. (a) Electrical activation ratio for $In_{2-2x}Zr_{2x}O_3$ films as a function of x. Here, the activation ratio was defined by the ratio of measured carrier density to the expected carrier density. (b) Hall mobility of $In_{2-2x}Zr_{2x}O_3$ films as a function of carrier density; each symbol is connected by lines from $x=0$ to $x=0.038$. The data of 930 nm thick film at $x=0.020$, and single-crystalline $In_{2-2x}Zr_{2x}O_3$ ($0 \leq x \leq 0.05$) films (after Ref. 10) are also shown as closed circles and open diamonds, respectively. The solid and dotted black lines are the calculated mobility due to ionized impurities (μ_I) assuming that the conducting carriers originate entirely from singly and doubly charged impurities, respectively.

higher mobility and lower carrier density, the transparency extended further into the NIR wavelength region as described below.

The behaviors of the electrical property as a function of x are quite in contrast to those of single-crystalline $In_{2-2x}Zr_{2x}O_3$ films, i.e., the carrier density followed the dotted line from $x=0$ to 0.005 and saturated at $x \sim 0.01$, while mobility increased first at $x=0.003$ and gradually decreased with increasing x. In order to discuss this, Figs. 5(a) and 5(b) summarize the activation ratio of free carriers as a function of x and relationship between Hall mobility and carrier density for the polycrystalline and single-crystalline $In_{2-2x}Zr_{2x}O_3$ films, respectively. Here, the activation ratio was defined by the ratio of measured carrier density to the expected carrier density, and the value over 1 might reflect the existence of additional donors by lattice defects (oxygen vacancies[12] or In interstitials[13]). Also, in Fig. 5(b) each symbol is connected by lines from $x=0$ to 0.038 for polycrystalline films and from $x=0$ to 0.05 for single-crystalline films. The dotted and solid black lines are the calculated mobility due to ionized impurities (μ_I) assuming that the conducting carriers originate entirely from doubly charged oxygen vacancies and singly charged Zr, respectively. The details of the expressions for μ_I can be found elsewhere.[14] Briefly, the theory of ionized impurity scattering,[15] which took into account the nonparabolicity of the conduction band,[14] was used in this study to express the μ_I for degenerate semiconductors, since the effects of the nonparabolicity of the conduction band[16] were observed strikingly for carrier density over approximately 1×10^{20} cm^{-3}.[17,18] Here, the values of effective mass derived by Fujiwara[19] for ITO was used and the value of static dielectric constant was taken as 9 for In_2O_3.[20]

For doped films, mobility is supposed to be dominated by the scattering of electrons from ionized and/or neutral impurities, such as singly charged Zr, oxygen vacancies, In or oxygen interstitials, defect complexes, and so on.[21] The scattering from grain boundary seems not to be dominant, because calculated mean-free path[22] of free electrons at the Fermi surface in semiconductors ranged from 2.0 to 11 nm for the film at $x=0.0032$ ($\rho=6.4 \times 10^{-3}$ Ω cm, N=3.1 $\times 10^{19}$ cm^{-3}, $\mu=32$ cm^2/V s), and $x=0.022$ ($\rho=2.6 \times 10^{-4}$ Ω cm, N=2.9 $\times 10^{20}$ cm^{-3}, $\mu=82$ cm^2/V s), respectively. The value was smaller than that of the crystalline size even in polycrystalline films as shown in Fig. 3(b). Regarding the single-crystalline films, nearly perfect activation ratio (≥ 0.9) was achieved at $x \leq 0.005$, and the mobility was close to the theoretical values dominated by singly charged ion scattering at a given carrier density (solid black line), indicating Zr behaves as a good donor impurity, i.e., one Zr^{4+} substitutes for one In^{3+}. Further increase in x resulted in the saturation of carrier density with a decrease in mobility, indicating the increase of electrically inactive Zr in In_2O_3, which did not generate free carriers and was considered to have negative effects on electron transport in terms of producing additional scattering centers.[21] On the other hand, for polycrystalline films, Zr did not activate in the first stage, and the carrier density decreased with increase in mobility. The results indicate that Zr in In_2O_3 reduces the numbers of donor-type scattering centers. Indeed, the residual carrier density of the undoped sputtered film was much larger than that of the single-crystalline film, indicating the existence of many donor-type lattice defects (oxygen vacancies[12] or In interstitials[13]). Also, the slope of the increase in mobility as a function of carrier density as shown in Fig. 5(b) is similar to that of the calculated mobility scattered by ionized impurity as shown in solid and dashed lines. The mechanisms of the reduction of donor-type lattice defects by Zr-doping cannot be discussed only from these data; however, interactions between substitutional Zr and oxygen (including oxygen vacancies and interstitial oxygens) may influence them. In the second stage, the activation ratio gradually increased from 16% to 43% with increasing x, and the mobility exceeded the theoretical value dominated by scattering from doubly charged ions (dotted black line) and approached the value dominated by scattering from singly charged ions (solid black line) at a given carrier density, indicating that most carriers originated from singly charged Zr, and multicharged donor-type defects (oxygen vacancies) and neutral defects are reduced with increasing x. Note that the sputtered films ($0.014 \leq x \leq 0.022$) positioned at the extrapolated line for the single-crystalline films ($0.003 \leq x \leq 0.01$) to a carrier density of over 10^{20} cm^{-3}, as shown by a gray thick line in Fig. 5(b). The results also support that the dominant scattering mechanism of free electrons is not grain boundary but lattice defects inside grains. In the third stage, further increase in x led to an increase in electrically inactive Zr in In_2O_3, which did

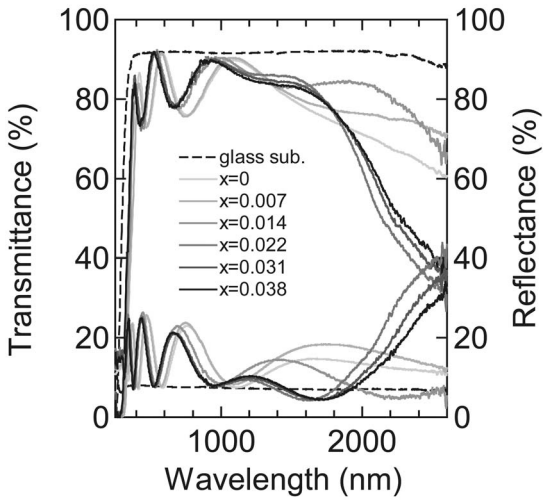

FIG. 6. Transmittance and reflectance spectra of $In_{2-2x}Zr_{2x}O_3$ polycrystalline films on glasses. The spectra of the glass are also shown as dotted lines.

not generate free electrons, as observed in single-crystalline films. The electrically inactive Zr in In_2O_3 lattice is considered to be an additional scattering center, which might lead to decrease in mobility and/or donor compensation, as mentioned above.

Figure 6 shows transmittance and reflectance spectra of the sputtered $In_{2-2x}Zr_{2x}O_3$ films and the glass substrate. All the films were transparent in the visible wavelength region, and a decrease in transmittance in the NIR wavelength region was observed due to the free-carrier absorption. The onset wavelength, at which transmittance began to decrease, varied with x. Note that the film at $x=0.022$, which showed similar resistivity ($2.6\times10^{-4}\ \Omega$ cm) to commercially available ITO films, showed high transparency ($\geq 80\%$) up to approximately 1700 nm. Due to the substantially higher mobility ($82\ cm^2/V\ s$) and lower carrier density ($2.9\times10^{20}\ cm^{-3}$), the transparency extended further into the NIR wavelength region and the magnitude of the free-carrier absorption reduced compared to commercially available ITO films.

IV. CONCLUSION

Transparent conductive polycrystalline $In_{2-2x}Zr_{2x}O_3$ ($0\leq x\leq 0.038$) films were deposited on glasses by rf magnetron cosputtering method using In_2O_3 and Zr-doped In_2O_3 ceramic targets. High mobility of over $80\ cm^2/V\ s$ was achieved under a carrier density of $1.3-2.9\times10^{20}\ cm^{-3}$ at Zr concentrations (x) of 0.014–0.022, and the film at $x=0.022$ showed similar resistivity ($2.6\times10^{-4}\ \Omega$ cm) to commercially available ITO. Analysis of the relationship between the values of Hall mobility and carrier concentration indicates that most carriers in the $In_{2-2x}Zr_{2x}O_3$ ($0.014\leq x\leq 0.022$) films originated from singly charged Zr, and multicharged donor-type defects (oxygen vacancies) and neutral defects are reduced by Zr-doping. Reflecting the high mobility and the low carrier density, the transparency extended further into the NIR wavelength region and the magnitude of the free-carrier absorption reduced compared to commercially available ITO films. Hence, $In_{2-2x}Zr_{2x}O_3$ films could have a performance advantage for applications that require high transparency in the NIR wavelength region, such as thin-film solar cells and photodetectors.

[1] R. Groth, Phys. Status Solidi **14**, 69 (1966).
[2] Y. Meng, X. Yang, H. Chen, J. Shen, Y. Jiang, Z. Zhang, and Z. Hua, Thin Solid Films **394**, 218 (2001); J. Vac. Sci. Technol. A **20**, 288 (2002).
[3] Y. Yoshida, T. A. Gessert, C. L. Perkins, and T. J. Coutts, J. Vac. Sci. Technol. A **21**, 1092 (2003).
[4] C. Warmsingh, Y. Yoshida, D. W. Readey, C. W. Teplin, J. D. Perkins, P. A. Parilla, L. M. Gedvilas, B. M. Keyes, and D. S. Ginley, J. Appl. Phys. **95**, 3831 (2004).
[5] A. E. Delahoy and S. Y. Guo, J. Vac. Sci. Technol. A **23**, 1215 (2005).
[6] M. F. A. M. van Hest, M. S. Dabney, J. D. Perkins, D. S. Ginley, and M. P. Taylor, Appl. Phys. Lett. **87**, 032111 (2005).
[7] P. F. Newhouse, C.-H. Park, D. A. Keszler, J. Tate, and P. S. Nyholm, Appl. Phys. Lett. **87**, 112108 (2005).
[8] X. Li, W. Miao, L. Huang, Z. Zhang, and Z. Hua, J. Vac. Sci. Technol. A **24**, 1866 (2006).
[9] A. A. Selvan, Y. Li, S. Guo, and A. E. Delahoy, in *Proceedings of the 19th European PVSEC*, Paris, France (WIP, Munich, 2004), pp. 1346–1351.
[10] T. Koida and M. Kondo, Appl. Phys. Lett. **89**, 082104 (2006).
[11] T. Koida and M. Kondo, J. Appl. Phys. **99**, 123703 (2006).
[12] J. H. W. de Wit, J. Solid State Chem. **20**, 143 (1977).
[13] A. J. Rosenberg, J. Phys. Chem. **64**, 1143 (1960).
[14] T. Pisarkiewicz, K. Zakrzewska, and E. Leja, Thin Solid Films **174**, 217 (1989).
[15] R. B. Dingle, Philos. Mag. **46**, 831 (1955).
[16] R. T. Bate, R. D. Baxter, F. J. Reid, and A. C. Beer, J. Phys. Chem. Solids **26**, 1205 (1965).
[17] Y. Ohhata, F. Shinoki, and S. Yoshida, Thin Solid Films **59**, 255 (1979).
[18] A. K. Kulkarni and S. A. Knickerbocker, J. Vac. Sci. Technol. A **14**, 1709 (1996).
[19] H. Fujiwara and M. Kondo, Phys. Rev. B **71**, 075109 (2005).
[20] I. Hamberg and C. G. Granqvist, J. Appl. Phys. **60**, R123 (1986).
[21] G. Frank and H. Köstlin, Appl. Phys. A: Solids Surf. **27**, 197 (1982).
[22] H. Hoffmann, J. Pickl, M. Schmidt, and D. Krause, Appl. Phys. **16**, 239 (1978).